J Mater Sci (2008) 43:123–131
DOI 10.1007/s10853-007-2122-8

Orientation relations between carbon nanotubes grown by chemical vapour deposition and residual iron-containing catalysts

Che-Yi Wen · Chun-Chia Huang · Huy-Zu Cheng · Hong-Yang Lu

Received: 15 January 2007 / Accepted: 21 August 2007 / Published online: 29 September 2007

Abstract Orientation relationships between the growth direction of carbon nanotubes and encapsulated residual iron-containing particles have been determined using transmission electron microscopy. The nanotubes that are prepared by Fe-catalysed chemical vapour deposition on sol–gel $Fe(NO_3)_3$-tetraethyl orthosilicate substrates are the helical multiwall type. Nanoscale particles of both the low-temperature α-Fe (ferrite) and high-temperature γ-Fe (austenite) were found in the cavity of the carbon nanotubes with $\langle 001\rangle_\alpha$, $\langle 011\rangle_\alpha$ and $\langle 110\rangle_\gamma$ parallel to the tube growth direction, respectively. Cementite Fe_3C, the most abundant Fe-containing phase in present samples was also found to be entrapped in nanotubes with $[100]_{Fe_3C}$ or $[101]_{Fe_3C}$ parallel to the tube axis. The metastable retention of γ-Fe particles at room temperature is ascribed to the strain energy induced at the particle-nanotube interface due to volume expansion upon the γ- $\rightarrow$ α-Fe phase transformation. The decomposition of initially high aspect-ratio, rod-shape particles into a string of ovulation, while encapsulated in carbon nanotubes is accounted for by the Rayleigh instability. Ovulation leading to reduced particle size has also contributed to increase the surface energy term that counterbalances the total free energy change of phase transformation from γ- to α-Fe and further aids to the metastable retention of γ-Fe.

C.-Y. Wen · C.-C. Huang · H.-Y. Lu (✉)
Centre for Nanoscience, Institute of Materials Science and Engineering, National Sun Yat-Sen University, Kaohsiung 80424, Taiwan
e-mail: hyl@mail.nsysu.edu.tw

H.-Z. Cheng
Department of Materials Engineering, I-Shou University, Kaohsiung 84008, Taiwan

Introduction

Carbon nanotubes (CNTs) are synthesized by various growth techniques using metal particles as growth catalysts [1–4]. Further modifications on arc-discharge [5, 6] have led to other techniques of laser evaporation [7] and plasma-enhanced chemical vapour deposition (PECVD) [8] that offered the feasibility of mass production of CNT with controlled structure and reduced cost [8]. Thermal CVD for preparing CNT with uniformity, high yield and low cost [8] is a relatively simple process rendering great advantage, particularly for use in a laboratory scale production. When catalysts, usually iron, cobalt and nickel, are added to improve the reaction, the process is termed, accordingly, catalyst (C) CVD. Most of CNT prepared by PECVD using Fe as growth catalyst [4, 8] have residual catalyst particles that remained inside the cavity or at the tip of CNT after synthesis. Although the catalysts were usually removed [9], subsequently, in order to retain the original properties of CNT, their presence inside CNT was thought to be directly connected to the growth mechanism [4, 10]. Two distinctive growth modes have been recognized in CCVD [8]: (a) growing from tip, the tip mode, and (b) growing from base, the base mode. A mechanism suggesting growth from the tip involving Fe and carbon decomposed from Fe_3C particles at processing temperatures was proposed [4] with convincing experimental observations.

Studies of multiwall (MW) CNTs grown by CVD have reported [10] the orientation relationships between Fe and the nanotubes. While α-Fe oriented in $\langle 001\rangle_\alpha$ and $\langle 111\rangle_\alpha$, and γ-Fe along $\langle 110\rangle_\gamma$ along with the physical tube axis were determined from electron diffraction, no such relationships were reported for Fe_3C found predominantly at the tip of nanotubes [4, 10]. The metastable retention of γ-Fe particles was attributed [10] to decreasing aspect ratio (with shortened length of the rod-shape particles), melting of the catalyst particles due to small sizes, and high elastic modulus of CNT confining the nanoparticles. Understanding the residual phases in CNT, the characteristic microstructure and crystallographic relationships are important both for the modification of physical properties and the feasibility of mass production using CCVD technique. It would assist not only in designing the composition of the substrates where catalyst precursors are embedded, but also in incorporating ferromagnetic α-Fe catalyst particles to modify magnetic properties [11, 12].

In this study, the crystalline phases of MWCNT samples prepared by CCVD adopting sol–gel SiO_2 substrates embedded with iron has been analysed systematically. It is reported here the crystallographic orientation relationships between carbon nanotubes and the growth catalysts of α-, γ-Fe, and Fe_3C formed during deposition using transmission electron microscopy (TEM). Although crystallographic orientation relationships similar to those reported before [4, 10] are determined and confirmed, the metastable retention of high temperature γ-phase is discussed in terms of end-point thermodynamics by considering the strain energy induced due to the volume expansion accompanying with the γ- → α-Fe phase transformation. Ovulation or spheroidisation of Fe particles confined in CNT is explained in terms of Rayleigh instability.

Experimental procedures

A CVD horizontal flow reactor, incorporating a silica-tube furnace and using N_2 as carrier gas, similar to those reported before [1–3] was adopted for growing CNT. Nanotube samples were grown on a Fe-containing sol–gel SiO_2 layer prepared by using precursors of $Fe(NO_3)_3 \cdot 9H_2O$ and tetraethyl orthosilicate (TEOS, $Si(C_2H_5)_4$), mixed in absolute alcohol (>99%) to make a solution. After gelation, it was coated on a silica glass substrate used as catalyst support. All chemicals supplied by Fluka Chemie of Buchs, Switzerland were the reagent grade. Samples were prepared by heating the gel-coated substrates in three successive steps. The SiO_2 gel was calcined at 450 °C for 5 h, followed by reduction of iron oxides to Fe in $H_2(g)$ at 550 °C for 2 h, acetylene (C_2H_2) was then passed through the reaction chamber with a silica-tube furnace preheated to 750 °C for 0.5 h in a $N_2(g)$ environment.

Crystalline phases in samples scraped from the glass substrate were analysed using X-ray diffractometry (XRD). A Siemens D5000 XRD (Karshrule, Germany) with Cukα radiation operating at 40 kV/30 mA was used. Microstructure was analysed by scanning electron microscopy (SEM) using a JEOL™ 6400 (Tokyo, Japan) operating at 20 kV equipped with X-ray dispersive energy spectrometry (EDS; Link Systems, Oxford Instruments, Oxford, UK) and TEM using a JEOL™ AEM 3010 operating at 200 or 300 kV. Specimens were prepared from CNT samples scraped from glass substrate; they were dispersed in absolute alcohol, ultrasonicated before pipetted and settled in holey carbon grids for TEM observations.

Results

General observation

Figure 1 shows the XRD trace of CNT samples. A mixture of CNT with Fe_2SiO_4 (fayalite of the olivine group [13], JCPDS 34-0178) and Fe_3C (cementite, JCPDS 35-0772) were obtained and those reflection peaks were assigned accordingly. Both Fe_2SiO_4 and Fe_3C are orthorhombic but with different space group assignment of *Pmnb* and *Pnma* (both being No. 62) in JCPDS files, respectively. The existence of $(111)Fe_2SiO_4$ formed from reaction between catalyst and silica gel upon calcination was checked for consistency from three samples. Most XRD measurements gave interlayer spacing of approximately 0.344 nm, e.g. [14, 15], which is assigned to $(0002)_{CNT}$ (as indicated in Fig. 1). The (0002) reflection peak of CNT corresponds similarly to $d_{0002} \sim 0.335$ nm between grapheme layers at $2\theta \approx 26.23°$ of JCPDS 75-1621 for graphite.

Cementite Fe_3C appears to be the predominant Fe-containing phase in CVD samples since neither γ-Fe (with {111} at $2\theta = 42.76$ °) nor α-Fe (with {110} at $2\theta = 44.66$ °) was registered in XRD traces. The absence of relevant reflection peaks from the XRD patterns suggests that CNT contains iron of <3 wt.%.

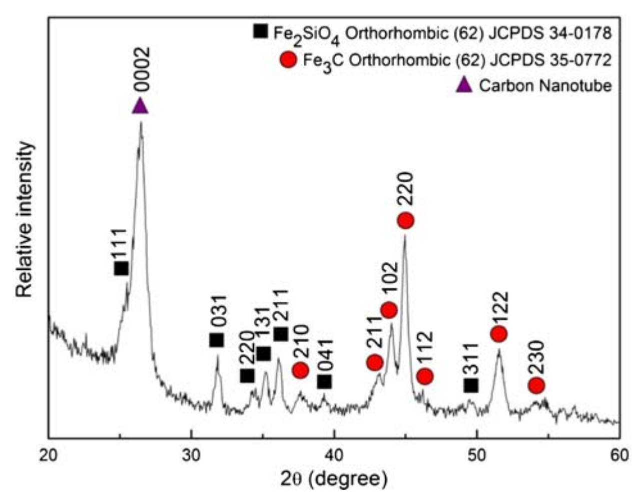

Fig. 1 Representative XRD trace of CNT samples containing two major residual phases of Fe_2SiO_4 and Fe_3C

Clusters of CNT varying in tube diameter are shown in Fig. 2a. Backscattered electron image (BEI) in Fig. 2b reveals the atomic contrast of Fe-containing phase(s) (corresponding EDS spectrum shown in the inset) entrapped in the cylindrical cavity of CNT. Such scattered grains in other CNT's of smaller diameters might also be discerned from Fig. 2b, as indicated.

Analysis by TEM

All nanotubes examined here are the multiwall type and most of them have diameters <200–100 nm. Nanotubes were easily damaged by electron irradiation, limiting the exposure time or lowering the accelerating voltage was often necessary during observation.

For γ-Fe particles encapsulated in nanotube cavity

A string of Fe particles confined within the cylindrical cavity of CNT is discerned in Fig. 3a. Two larger ones of rod-like shape appearing dark in BF image are designated A and B. Particle A was tilted to approximately the Bragg diffraction condition whose corresponding SADP indexed to Z = $[011]_\gamma$ of fcc γ-Fe ($Fm\bar{3}m$, No. 225) is shown juxtaposed. All odd or all even reflections are allowed, e.g. 200 and $02\bar{2}$, while reflections with mixed indices are forbidden, e.g. 100 and $01\bar{1}$, for fcc. Extra diffraction rings were artefacts caused by holey carbon film of the supporting grid. Four other γ-Fe particles of much smaller in size, indicated by arrows in Fig. 3a, were located between A and B in approximately equal spacing.

The $(02\bar{2})$ plane of γ-Fe is parallel to (0002) of CNT, i.e. $(0\bar{2}2)_\gamma \| (0002)_{CNT}$, as indicated in SADP of Fig. 3a for region A and the trace of plane (0002) is also shown in Fig. 3c. The corresponding SADP of region B (Fig. 3b) is also indexed to Z = $[122]_\gamma$ of γ-Fe. Regardless of multiple helical angles [15, 16], the (0002) spots are coincident and remain the same in SADP [17], as indicated. Streaking of spots perpendicular to the tube axis (of e.g. $\langle 10\bar{1}0 \rangle$ for zigzag) representing the range of helical α-angle in MWCNT [15, 17, 18] was not detected. In fact, no reflections other than (0002) and (0004) were detected. The broadened rings, indicated in Fig. 3a are due to amorphous materials present in holey carbon grid or in sample.

Nevertheless, the growth direction, i.e. the longer (tube) axis of CNT although inclining an angle between the prismatic directions of $\langle 2\bar{1}\bar{1}0 \rangle$ (armchair type of helicity $\alpha = 30°$) or $\langle 10\bar{1}0 \rangle$ (zigzag type of helicity $\alpha = 0°$) is perpendicular to $[100]_\gamma$ of γ-Fe. The C–C bonds are normal to the tube axis for the armchair type while parallel for the zigzag type. For helical tubes, the α-angle describing the helicity of CNT lies between the two extremes and the growth direction would incline such an angle to the C–C bonds.

Several γ-Fe particles found in regions C and D, as indicated by in Fig. 4a, have also grown along the prismatic directions of CNT. The growth (tube) direction is determined, adopting the technique reported by Kim et al. [10], by the cross product $\mathbf{g}_1 \times \mathbf{g}_2$, two **g**-vectors, $\mathbf{g}_1$ and $\mathbf{g}_2$ of the reflection planes in γ-Fe that lying parallel to (0002) of CNT were found by tilting CNT along its tube direction, i.e. perpendicular to reciprocal direction $\mathbf{0001}^*_{CNT}$. It is shown in Fig. 4a, b and c for γ-Fe particle in region C (indicated in Fig. 4d). The (200) plane of both particles in regions A (Fig. 3c) and C (Fig. 4a) are aligned in parallel to (0002) of CNT, i.e. $(200)_\gamma \| (0002)_{CNT}$ from Z = $[011]_\gamma$ as evidenced from corresponding SADP in Fig. 4b for the γ-Fe particle in region C. The streaking at the 0002 spot has arisen from slightly different orientation of the tube axis due to strains in region C. The tube growth direction of $[011]_\gamma$, similar to that reported by Kim et al. [10], is determined on the basis of three **g**-vectors representing parallel planes of $(200)_\gamma \| (0002)_{CNT}$ from Z = $[011]_\gamma$ (Fig. 4b), $(\bar{5}\bar{1}\bar{1})_\gamma \| (0002)_{CNT}$ from Z = $[\bar{2}55]_\gamma$ (Fig. 4c) and $(311)_\gamma \| (0002)_{CNT}$ from Z = $[\bar{2}33]_\gamma$ (Fig. 4d).

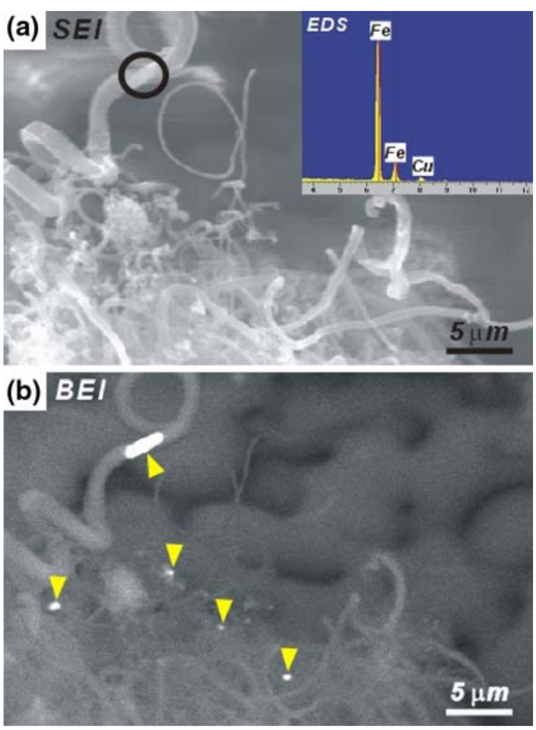

Fig. 2 CNT with Fe-containing phases encapsulated, (**a**) SEI with corresponding EDS spectrum in the inset, and (**b**) BEI showing atomic contrast (SEM)

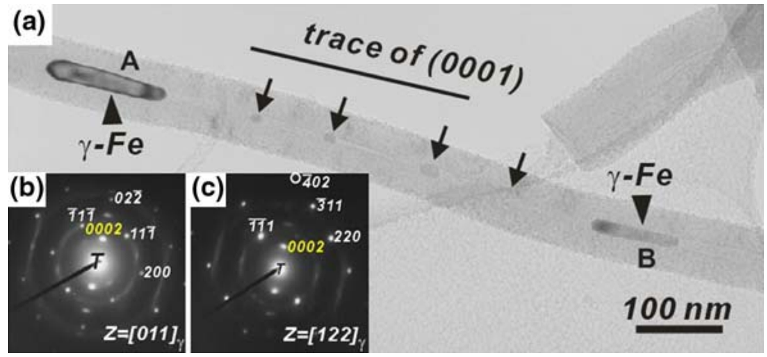

Fig. 3 (a) A string of γ-Fe particles with higher magnification shown in the inset, corresponding SADP of (**b**) Z = $[011]_\gamma$ for framed region A, and (**c**) Z = $[122]_\gamma$ for region B (TEM)

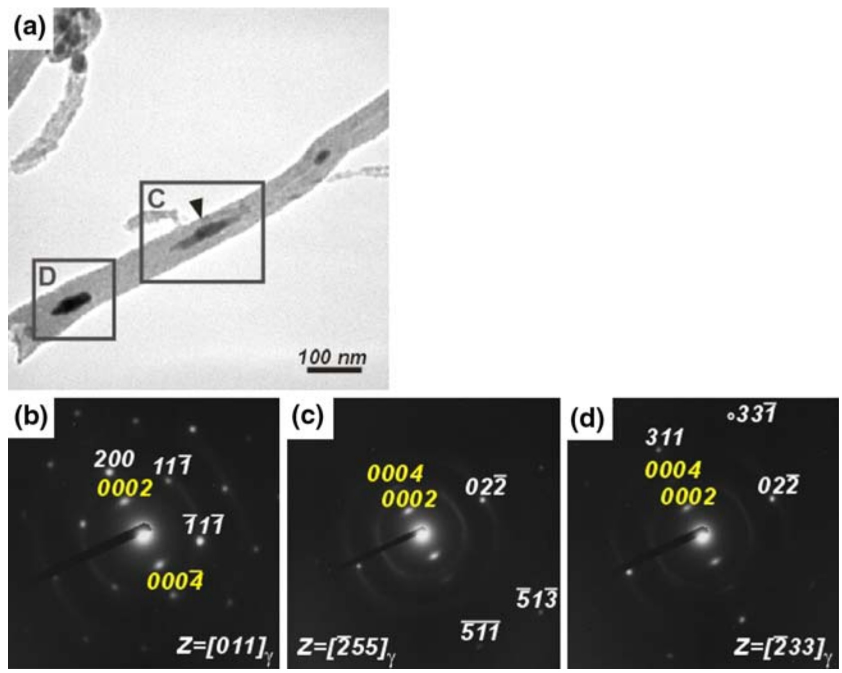

Fig. 4 (**a**) γ-Fe particles in framed regions C and D with higher magnification shown in the inset, corresponding SADP of (**b**) Z = $[011]_\gamma$, (**c**) Z = $[\bar{2}55]_\gamma$ and (**d**) Z = $[\bar{2}33]_\gamma$ for framed region C (TEM)

Region D at the end of CNT appearing to have broken off also exhibits similar orientation relationships.

For α-Fe particles encapsulated in nanotubes

α-Fe particles, however, are situated within the cavity and at the tip of CNT. Figure 5a reveals a cluster of CNT in which α-Fe particles (region E) are encapsulated in many locations. A string of α-Fe particles (indicated by arrow) could be seen from a higher magnification shown in the inset. Almost randomly oriented CNT, as indicated by the diffuse arc of (0002) in corresponding SADP, is shown in Fig. 5b with SADP of α-Fe indexed to Z = $[111]_\alpha$ from the $1\bar{1}0$ spots that are forbidden for fcc γ-Fe but characteristic to the bcc structure of α-Fe have emerged. The arc from several α-Fe particles, however, has prevented an unambiguous determination of orientation relationships between the CNT and α-Fe at its tip. Nevertheless, the (0002) planes are parallel to $\{1\bar{1}0\}_\alpha$ of α-Fe, as indicated in Fig. 5b.

Strain contrast observed along the long axis direction, as indicated by filled arrows in Fig. 6a, suggests that the multiwall CNT contains defects of, e.g. stacking faults or dislocations [16]. Orientation relationship is successfully determined for α-Fe encapsulated in CNT (region F containing two particles shown in Fig. 6a) with corresponding SADP using a similar technique. Parallel planes having the relation: $(\bar{2}11)_\alpha \| (0002)_{CNT}$ from Z = $[111]_\alpha$. Tilting about the tube axis gives $(\bar{2}22)_\alpha \| (0002)_{CNT}$ from Z = $[211]_\alpha$ (Fig. 6b) and $(011)_\alpha \| (0002)_{CNT}$ from Z = $[100]_\alpha$ (Fig. 6c). The growth direction of CNT perpendicular to $[011]_\alpha$ is determined accordingly.

Another α-Fe particle (Fig. 6d with corresponding SADP in the inset) having parallel crystal planes of $(\bar{1}01)_\alpha \| (0002)_{CNT}$ and $(\bar{4}02)_\alpha \| (0002)_{CNT}$ is determined to have its growth direction perpendicular to $[0\bar{1}0]_\alpha$ similar to that reported before [10].

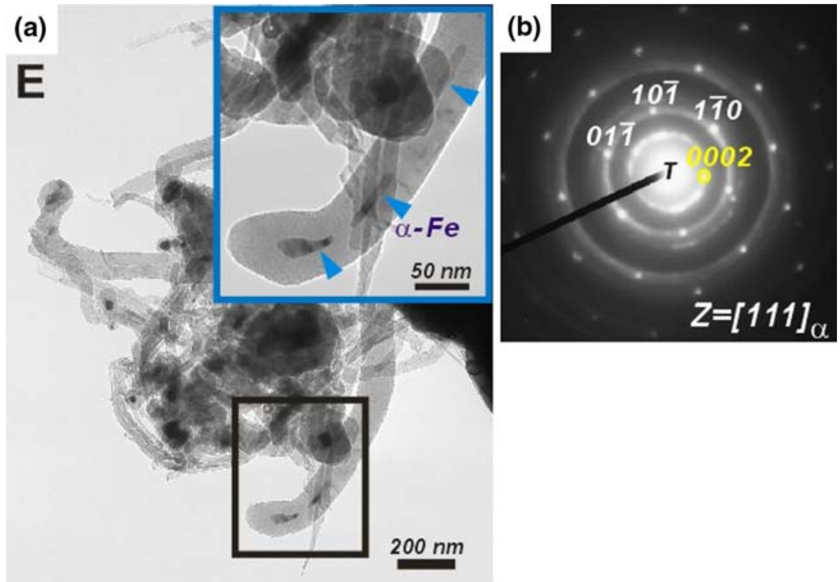

Fig. 5 (**a**) Cluster of CNT encapsulated with α-Fe particles (region E) with higher magnification shown in the inset, corresponding SADP of (**b**) Z = $[011]_{\alpha}$ (TEM)

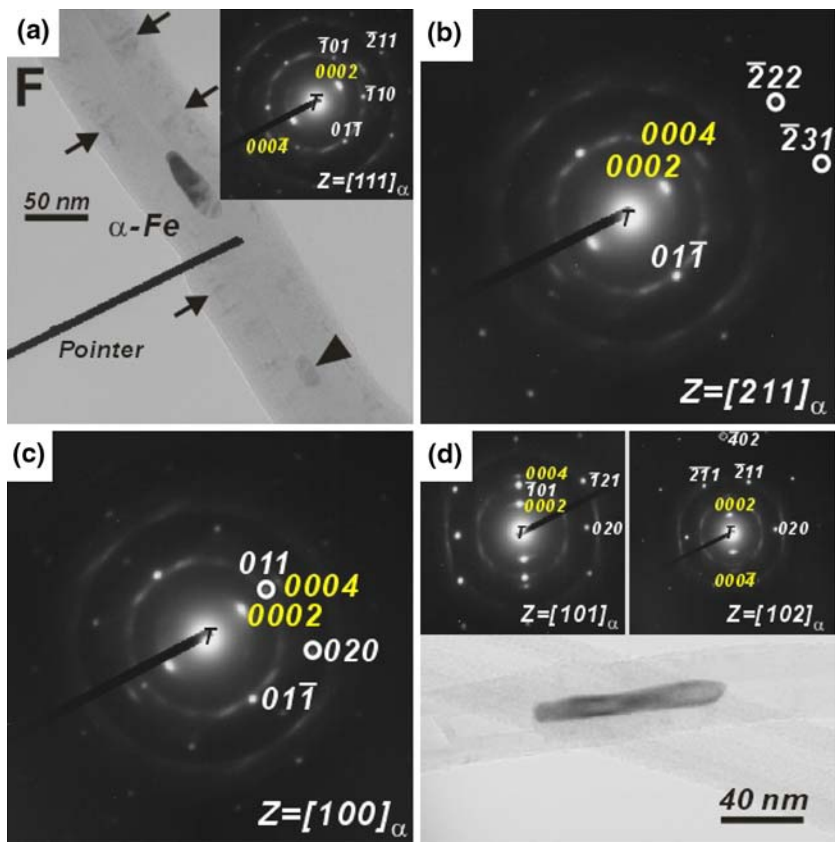

Fig. 6 (**a**) α-Fe particle in framed region F with corresponding SADP of Z = $[111]_{\alpha}$, (**b**) Z = $[211]_{\alpha}$, (**c**) Z = $[100]_{\alpha}$ and (**d**) another α-Fe rod with corresponding SADP shown in the inset (TEM)

For α- and γ-Fe particles both encapsulated in nanotube cavity

The co-existence of both α- and γ-Fe particles in a nanotube cavity is shown in the framed regions of G and H in Fig. 7a along the growth direction. Corresponding SADP for α-Fe are shown in Fig. 7c where curved tube is evident from the arc of (0002), as indicated. Similarly, parallel planes of $(0\bar{2}0)_{\alpha} \| (0002)_{CNT}$ (Fig. 7b and c) permit determination of tube axis to $[\bar{1}01]_{\alpha}$, this is consistent with that derived from Fig. 6a–c. Tube curving increases towards tip end (region H) as evidenced by the larger arc in corresponding SADP (Fig. 7a versus Fig. 7c) where nanotube grows along the $[101]_{\gamma}$ direction of γ-Fe similar to that in

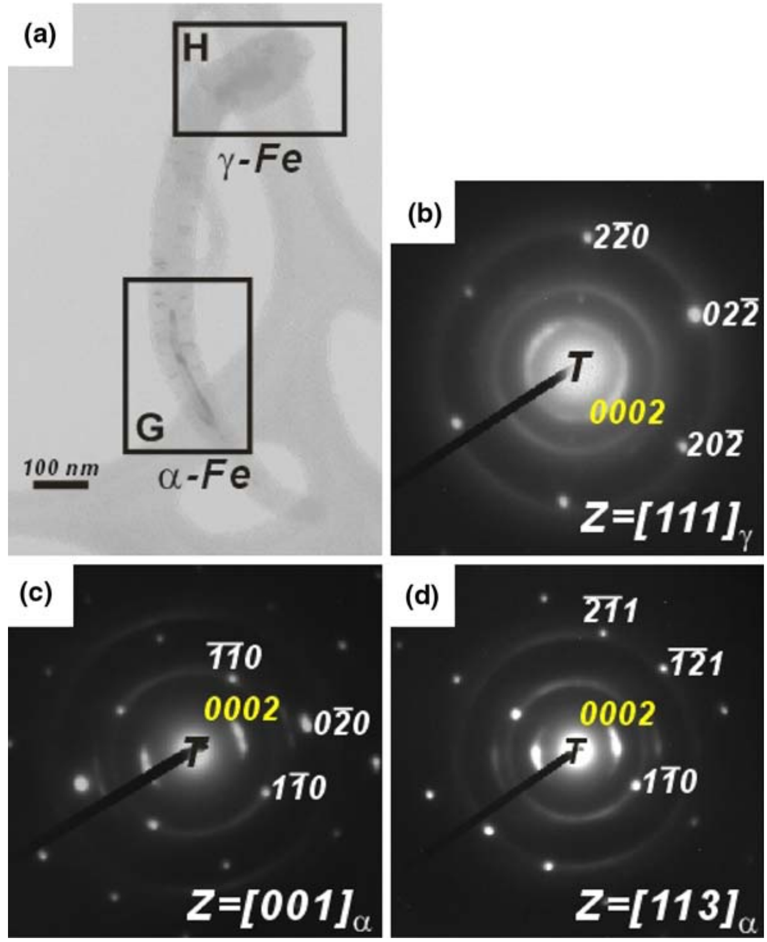

Fig. 7 (**a**) α-Fe and γ-Fe particle in framed region G and H respectively encapsulated in one CNT with corresponding SADP of (**b**) $Z = [111]_{\gamma}$, (**c**) $Z = [001]_{\alpha}$ and (**d**) $Z = [113]_{\alpha}$ (TEM)

Fig. 3. Nevertheless, the diffuse arc due to curving (Fig. 7c and d) has made the determination of growth direction parallel to $[\bar{1}01]_{\alpha}$ ambiguous.

For Fe_3C particles at tube tip

Considerable beam damage has occurred to this particular nanotube containing two rods of ~300–400 nm long in its cavity (Fig. 8a). The particles were confirmed of Fe_3C by electron diffraction, shown in Fig. 8b and c are corresponding SADP for region I only. Parallel crystal planes between Fe_3C and CNT of $(010)Fe_3C||(0002)_{CNT}$ (Fig. 8b) and $(05\bar{1})Fe_3C||(0002)_{CNT}$ (Fig. 8c) are found. The growth direction of $[100]Fe_3C$ is again determined by the cross product of $\mathbf{g}_1 = 020$ and $\mathbf{g}_2 = 05\bar{1}$.

Another cemenite rod was found (shown in Fig. 9a) and its orientation relationship with CNT was analysed. Necking near one end, as indicated, suggests that ovulation along tube axis is imminent. Parallel planes of $(202)Fe_3C||(0002)_{CNT}$ (Fig. 9b) and $(212)_{Fe3C}||(0002)_{CNT}$ (Fig. 9c) indicated in corresponding SADP shown in juxtaposition has enabled to determine the growth direction of CNT along the axial direction parallel to $[\bar{1}01]Fe_3C$.

Discussion

Inclined (0002) planes and curving of nanotubes

Reciprocal space construction suggests that the reciprocal lattice points for a non-helical tube are circles [15–19]. Therefore, the (0002) planes registered correspondingly as the 0002 spots are usually observed [15, 16] from a straight CNT as shown for example in Fig. 3b. However, multiwall tubes are mostly helical and the C–C bonds are inclining an α-angle of 0–30° with the tube axis. Although the helicity of MWCNT should have been registered as streaks on the reflections of $\{10\bar{1}0\}$ and $\{2\bar{1}\bar{1}0\}$ [15–19], such reflections did not appear in all SADP examined.

The diffuse arcs usually indicate grains in a polycrystalline aggregate that exhibit preferred crystallographic orientation with correspondingly an angle of rotation about the zone axis. Here, the arc in 0002 is due to the changing of axial directions in curved nanotubes. This is best

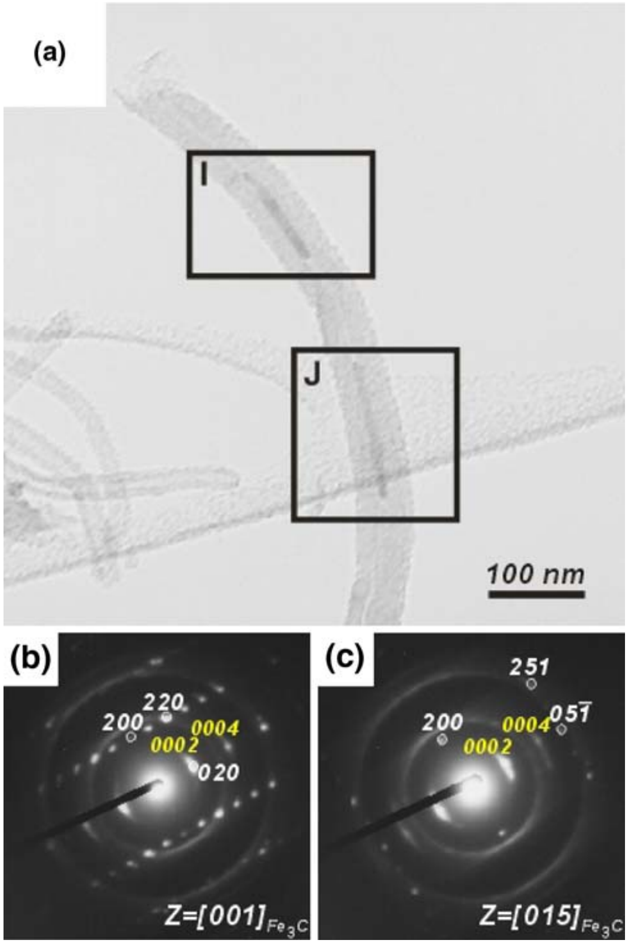

Fig. 8 (**a**) Two Fe_3C entrapped in curved CNT with corresponding SADP of (**b**) Z = $[001]_{Fe_3C}$, and Z = $[015]_{Fe_3C}$ (TEM)

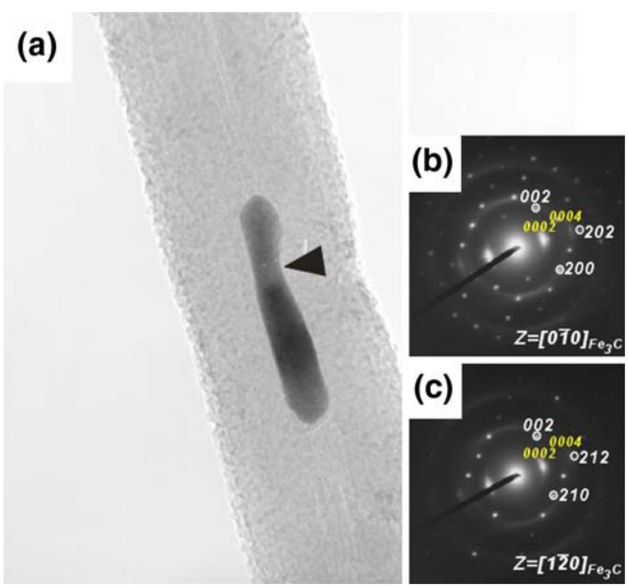

Fig. 9 An entrapped Fe_3C particle (**a**) with corresponding SADP of (**b**) Z = $[0\bar{1}0]_{Fe_3C}$, and (**c**) Z = $[1\bar{2}0]_{Fe_3C}$ shown in juxtaposition (TEM)

exemplified by tubes clustered in Fig. 5a resembling a polycrystalline aggregate of random orientations.

Relatively straight nanotube as in Fig. 4a does not have an arc on the 0002 reflection spot (Fig. 4b). The tube curved at tip (Fig. 7a) is also registered by an arc (Fig. 7c of a small arc and Fig. 7b of a larger one) again due to change in the growth direction. Such a bend along CNT may be analogously regarded as grain boundary. Unlike the model proposed by Kim et al. [4, 10], Fe_3C was not found at the tip.

Metastable retention of γ-Fe

All Fe-containing particles appear as single crystals [4, 10], unlike a mixture of crystalline phases from Mössbauer studies [20]. The fact that the stable phase field of (pure) γ-Fe lies between 1396 ° and 912 °C [21] suggests the γ-Fe particles found here have been retained metastably at room temperature [4, 10]. They are formed in the stable phase field during CVD deposition at 750 °C exceeding the eutectoid temperature 727 °C of the Fe–C binary system, should then phase transform to α-Fe upon cooling to room temperature. However, these particles may have compositions lied in four phase fields depending on carbon content, and they are accordingly: (i) α-phase, (ii) $\alpha + \gamma$ mixture, (iii) γ-phase, and (iv) γ + C or $\gamma + Fe_3C$ upon increasing solute (i.e. carbon) content.

Phase transition of γ- to α-Fe is accompanied with a volume expansion of ~9% [22], similar to that of ~3.0–4.9% in the tetragonal (t) → monoclinic (m) phase transformation in ZrO_2. The metastable retention of t-ZrO_2 [23–25] is attributed to the positive strain energy (ΔG_{strain}) from the matrix constraint of t-particles embedded in a rigid matrix (e.g. cubic (c)-ZrO_2 matrix). The positive ΔG_{strain} compensates for the combination of surface (ΔG_S) energy and volume (ΔG_V) energy in total free energy change (ΔG_{total}) upon phase transformation. Under insufficient matrix constraint, ΔG_{total} remains negative, phase transformation to α-Fe occurs thermodynamically according to the Fe–C binary equilibrium phase diagram. Arguing from end-point thermodynamics [25], when ΔG_{strain} from tube constraint becomes large enough to completely counterbalance the negative change in ΔG_{total}, and further results in positive total free energy change, i.e. $\Delta G_{total} > 0$, the phase transformation to α-Fe would then be suppressed and the high-temperature γ-Fe retained at room temperature.

The total free energy change for phase transition from γ- to α-Fe can be described by:

$$\Delta G_{total} = \Delta G_V + \Delta G_S + \Delta G_{strain} \quad (1)$$

Such phase transformation may either be thermal-, or stress-induced. For the former, phase transformation from γ- to α-Fe occurs athermally upon cooling when particles exceed a critical size ($r_{critical}$) For the latter, it ensues when the matrix constraints are relieved by externally applied tensile stress. The critical size of an unconstrained particles, in the absence of ΔG_{strain}, described in terms of ΔG_V and ΔG_S is: $r_{critical} = -3(\Delta G_V)/(\Delta G_S)$ [24, 25]. The surface energy term ΔG_S becomes positive if particle size was decreased below the critical value ($r_{critical}$) [23–26] and that further offsets the initially negative ΔG_{total}. Mechanical confinement would further augment to ΔG_S with a positive ΔG_{strain}, induced by the volume expansion, and compensates for the total free energy change ΔG_{total} of phase transformation. The ΔG_{strain} term in eq. (1) is supplemented additionally by positive ΔG_S from particle sizes $r < r_{critical}$ when Fe particles are confined in CNT cavity. The two effects of matrix constraint and reduced particle size would synergistically combine to counterbalance the negative ΔG_V and afford the metastable retention of the high temperature phases at room temperature, such as the metastable t-ZrO_2, c-$BaTiO_3$, and now γ-Fe. It is, therefore, suggested that γ-Fe particles are retained metastably due both to the constraint imposed physically by CNT and the reduced particle size by the Rayleigh decomposition (elaborated in the next section).

Growth mechanism and Rayleigh decomposition

The Fe_3C particles often located at the tip of CNT indicates a tip-mode growth mechanism [4] particularly when cementite is the predominant Fe-containing phase in the mixture (Fig. 1), although such a configuration was also detected (Fig. 8a) here but failed to reveal a close resemblance [4]. Kim et al.'s [4] model was based on Fe_3C particles that formed above 727 °C, the eutectoid temperature, decomposed on cooling subsequently to a mixture of γ-Fe (metastably retained) or α-Fe (transformed) and C. Independent of whether such a mechanism should have been dominating the growth of CNT by CVD, the iron particles trailing behind Fe_3C [4] is likely to have resulted from the Rayleigh instability [27] of a cylindrical rod, regardless of being solid or liquid [28, 29], or pore [30]. The driving force for cylindrical rods breaking up to ovulation is the decrease of interface energy [27–30], the energy between Fe rods and CNT. It is predicted [27] that instability occurs in a rod of infinite length and isotropic surface energy when($\lambda_o > 2\pi(r_o$, i.e. perturbation wavelength is greater than rod circumference, where r_o: rod radius, and λ_o: perturbation wavelength, when surface (interfacial) energy per unit volume is minimized by reducing the interfacial area. In a tip growth mode [4], the growing of CNT provides the necessary perturbation perpetually until Fe_3C is completely consumed.

Similar to Fe_3C, iron rods (of radius r_o) also become unstable and spheroidised to discrete particles when longitudinal perturbations (of wavelength λ_o) occur upon growing of CNT along its axial direction. Therefore, regardless of the crystalline phases of rods being Fe_3C, γ-Fe (Figs. 3a and 4a) or α-Fe (Fig. 5a), decomposing into a string of ovulations due to the Rayleigh instability to minimise the interface energy between CNT and Fe particles is observed. Of course, although the interfacial energy is minimised upon decomposition, confined in the cavity the strain energy (ΔG_{strain}) between CNT and γ-Fe particles would have been positive and large enough to facilitate metastable retention. Besides, reduction in particle sizes upon ovulation would have also contributed favourably to increase the surface energy term (ΔG_S) in the overall free energy change.

Conclusions

The crystallographic orientation relationships between CNT and the residual catalysts of γ-Fe, α-Fe, Fe_3C encapsulated in CNT are determined. The tube growth axis of multiwall CNT prepared by CVD is aligned with $\langle 110\rangle_\gamma$, $\langle 011\rangle_\alpha$, $\langle 001\rangle_\alpha$, and [100]$Fe_3C$ or [101]Fe_3C, respectively, but the physical axis does not coincide with either $\langle 2\bar{1}\bar{1}0\rangle_{CNT}$ or $\langle 10\bar{1}0\rangle_{CNT}$due to tube helicity. Although CNT samples were prepared by CCVD on sol–gel $Fe(NO_3)_3$-TEOS substrates, similar orientation relations determined before by Kim et al. were confirmed. Similar to t-ZrO_2 particles with matrix constraint where a critical size exists thermodynamically, the metastable retention of γ-Fe particles at room temperature is attributed analogously to the strain energy term induced by the $\sim$9% volume expansion upon the γ- → α-Fe phase transformation while confined in the CNT. Small particles of the residual phases encapsulated in CNT are likely to have decomposed from particles of an initially rod-like shape due to the Rayleigh instability where the interface area and energy is reduced. The ovulation of rod-shape particles, when the surface energy term is increased by reduced sizes, has further assisted on the metastable retention of γ-Fe.

Acknowledgements We thank the National Science Council of Taiwan for funding through contracts NSC 93-2216-E-110-015, 94-2216-E-110-004 and 95-2221-E-110-033.

References

1. Ren ZF, Huang ZP, Provencio PN (1998) Science 282:1105
2. Lee CJ, Kim DW, Lee TJ, Choi YC, Park YS, Lee YH, Choi WB, Lee NS, Park GS, Kim JM (1997) Chem Phys Lett 312:461
3. Pan ZW, Xie SS, Zhou WY, Wang G (1999) Chem Phys Lett 299:97
4. Kim H, Sigmund W (2000) Carbon 43:1743

5. Iijima S (1991) Nature 354:56
6. Ebbesen TW, Ajayan PM (2000) Nature 358:220
7. Qin LC, Iijima S (1997) Chem Phys Lett 269:65–71
8. AuBuchon JF, Daraio C, Chen LH, Gapin AI, Jin S (2005) J Phys Chem B Lett 109:24215
9. Strong KL, Anderson DP, Lafdi K, Kuhn JN (2003) Carbon 41:1477
10. Kim H, Sigmund W (2005) J Cryst Growth 276:594
11. Mühl T, Elefant D, Graff A, Kozhuhaova R, Leonhardt A, Mönch I, Ritschel M, Simon P, Groudeva-Zotova S, Schnider CM (2003) J Appl Phys 93:7894
12. Qiu J, Li Q, Wang Z, Sun Y, Zhang H (2006) Carbon 44:2565
13. Klein C, Hurlbut CS Jr (1993) Manual of Mineralogy, 21st edn. J. Wiley, New York, p 449
14. Zhou D, Fleming RM, Murphy DW, Chen CH, Haddon RC, Ramirez AP, Glarum SH (1994) Science 263:1744
15. Zhang XB, Zhang XF, Amelinckx S, van Tendeloo G, van Landuyt J (1994) Ultramicroscopy 54:237
16. Zhang XF, Zhang XB, van Tendeloo G, Amelinckx S, Op de Beeck M, van Landuyt J (1993) J Cryst Growth 130:368
17. Qin LC, Iijima S, Kataura H, Maniwa Y, Suzuki S, Achiba Y (1997) Chem Phys Lett 268:101
18. Bernaerts D, Zettl A, Chopra NG, Thess A, Smalley RE (1998) Solid Stat Comm 105:145
19. Liu M, Cowley JM (1994) Ultramicroscopy 53:333
20. Prados C, Crespo P, Gonzalez JM, Hernando A, Marco JF, Gancedo R, Grobert N, Terrones M, Walton RM, Kroto HW (2002) Phys Rev B 65:113405
21. Chipman J (1972) Metall Trans 3:55
22. Kim H, Kaufman MJ, Sigmund WM, Jacques D, Andrews R (2003) J Mater Res 18:1104
23. Heuer AH (1987) J Am Ceram Soc 70:689
24. Green DJ, Hannink RHJ, Swain MV (1989) Transformation toughening of ceramics. CRC Press, Boca Ranton, FL, p 17
25. Garive RC (1965) J Chem Phys 69:1238
26. Hsiang HI, Yen FS (1996) J Am Ceram Soc 79:1053
27. Lord Rayleigh (1878) Proc London Math Soc 4:4
28. Nichols FA (1976) J Mater Sci 11:1077
29. Cahn JW (1979) Script Metall 13:1069
30. Gupta TK (1978) J Am Ceram Soc 61:191